Published in final edited form as:

*ACS Chem Biol*. 2016 February 19; 11(2): 530–540. doi:10.1021/acschembio.5b00737.

# Mitochondrial Redox Opto-Lipidomics Reveals Mono-Oxygenated Cardiolipins as Pro-Apoptotic Death Signals

**Gaowei Mao**[†,‡,#], **Feng Qu**[†,‡,#], **Claudette M. St. Croix**[‡,§], **Yulia Y. Tyurina**[†,‡], **Joan Planas-Iglesias**[‖], **Jianfei Jiang**[†,‡], **Zhentai Huang**[†,‡], **Andrew A. Amoscato**[†,‡], **Vladimir A. Tyurin**[†,‡], **Alexandr A. Kapralov**[†,‡], **Amin Cheikhi**[†,‡], **John Maguire**[†,‡], **Judith Klein-Seetharaman**[‖], **Hülya Bayır**[†,‡,⊥], and **Valerian E. Kagan**[*,†,‡]

[†]Center for Free Radical and Antioxidant Health, University of Pittsburgh, Pittsburgh, Pennsylvania, United States

[‡]Departments of Environmental and Occupational Health, University of Pittsburgh, Pittsburgh, Pennsylvania, United States

[§]Center for Biological Imaging, University of Pittsburgh, Pittsburgh, Pennsylvania, United States

[‖]Division of Metabolic and Vascular Health, Medical School, University of Warwick, Coventry, United Kingdom

[⊥]Department of Critical Care Medicine, Safar Center for Resuscitation Research, University of Pittsburgh, Pittsburgh, Pennsylvania, United States

## Abstract

While opto-genetics has proven to have tremendous value in revealing the functions of the macromolecular machinery in cells, it is not amenable to exploration of small molecules such as phospholipids (PLs). Here, we describe a redox opto-lipidomics approach based on a combination of high affinity light-sensitive ligands to specific PLs in mitochondria with LC-MS based redox lipidomics/bioinformatics analysis for the characterization of pro-apoptotic lipid signals. We identified the formation of mono-oxygenated derivatives of C18:2-containing cardiolipins (CLs) in mitochondria after the exposure of 10-nonylacridine orange bromide (NAO)-loaded cells to light. We ascertained that these signals emerge as an immediate opto-lipidomics response, but they decay long before the commencement of apoptotic cell death. We found that a protonophoric uncoupler caused depolarization of mitochondria and prevented the mitochondrial accumulation of

[*]**Corresponding Author:** Phone: 412-624-9479. kagan@pitt.edu.

[#]These authors contributed equally to the work.

**Supporting Information**

The Supporting Information is available free of charge on the ACS Publications website at DOI: 10.1021/acschembio.5b00737. Supporting Information Tables S1 and S2, Figures S1–S12, Methods (PDF)

**Author Contributions**

G.M. designed and performed the cell experiments and cowrote the manuscript. Q.F. performed the MS analysis of PLs and cowrote the manuscript. C.M.S. performed live cell imaging experiments. Y.Y.T., V.A.T., and A.A.A. helped with the MS analysis of PLs. J.P. and J.K. performed the bioinformatics analysis. J.J., Z.H., A.A.K., and A.C. participated in the cell experiments. J. M. helped with writing the manuscript. H.B. formulated the idea, participated in the study design, and wrote the manuscript. V.E.K. formulated the idea, designed the study, and wrote the manuscript. All authors discussed the results and commented on the manuscript.

**Notes**

The authors declare no competing financial interest.

NAO, inhibited the formation of C18:2-CL oxidation product,s and protected cells from death. Redox opto-lipidomics extends the power of opto-biologic protocols to studies of small PL molecules resilient to opto-genetic manipulations.

## Graphical abstract

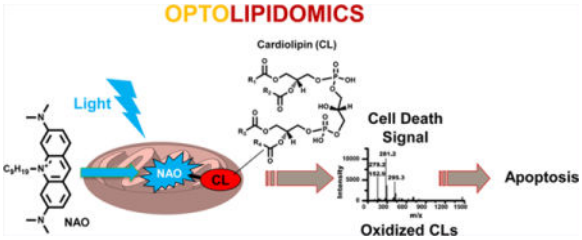


About a decade of opto-genetics has yielded numerous protocols for the expression of light-sensitive proteins that are effective in controlling and manipulating different aspects of cell metabolism and physiology.[1,2] This has resulted in a large array of potential biomedical applications from neurobiology/neurology to cardiovascular research, ophthalmology, urology, etc.[3–5] The utility of this approach for understanding the functions of small biomolecules, particularly identification of their signaling roles, has not been explored so far. One of the reasons is that, in contrast to macromolecules, selective expression and/or labeling of lipids with photosensitive chromophores and their targeted delivery to specific intracellular compartments has proven difficult.[6,7]

A notable exception is cardiolipin (CL)—an anionic phospholipid (PL) found almost exclusively in the inner mitochondrial membrane (IMM), the site of its biosynthesis by CL synthase (CLS).[8] The unusual CL's dimeric structure— combining two phosphatidic acid (PA) moieties linked via a glycerol backbone in the center—yields a highly hydrophobic yet dianionic hybrid molecule.[8,9] This unique structure of CL makes it indispensible for the proper organization of the IMM and many of its bioenergetic proteins as well as for several mitochondrial functions as both a central regulatory metabolic and cell death platform.[10] These specific features of CLs may be used for its selective postsynthetic targeting by opto-active probes, particularly those known to selectively accumulate on the matrix side of the IMM. Among the latter, 10-nonylacridine orange bromide (NAO), a fluorescent compound, capable of tight binding to CL,[11] has been introduced for the CL detection in mitochondria.[12] The presence of a positively charged quaternary ammonium and a hydrophobic nonyl moiety in NAO is believed to account for the enhanced selectivity of its interaction with CL—by far exceeding its binding to other mitochondrial anionic PLs including phosphatidylglycerol (PG), PA, and phosphatidylinositol (PI) as well as extramitochondrial phosphatidylserine (PS).[11]

Here, we have developed a novel redox opto-lipidomics approach in which selective light induced NAO-driven redox modifications of CLs were combined with high analytical resolution of LC-MS-based redox lipidomics and bioinformatics analysis. Membrane potential-driven selective accumulation of NAO into mitochondria resulted in light induced apoptosis accompanied by the generation of selectively mono-oxygenated CLs and

phosphatidylcholines (PCs) occurring immediately following light exposure. We further established that mitochondrial depolarization by a protonophoric uncoupler, carbonyl cyanide-4-(trifluoromethoxy)phenylhydrazone (FCCP), suppressed accumulation of these mono-oxygenated CL species and prevented light induced apoptosis. Our results establish the utility of opto-lipidomics as a new tool for studies of selective redox modifications of lipids, particularly mitochondrial CLs.

## RESULTS AND DISCUSSION

### LC-MS Characterization of Phospholidpidome of HeLa Cells

Using LC-MS, we have identified and quantified 146 PLs in HeLa cells, distributed between six major classes, including PC, phosphatidylethanolamine (PE), PI, PS, PG, and CL and different combinations of 18 fatty acids with chain lengths from 14 to 22 carbons and containing up to six double bonds (Table 1 shows compounds with an abundance of >1%; other compounds are in Supporting Information Table S1). All PLs were identified and quantified by high resolution mass spectrometry with mass accuracy <5 ppm and further confirmed by tandem mass spectrometry (MS/MS) fragmentation analysis. To minimize the cross inference between PL species, we employed solid phase extraction (SPE) and off-line two-dimensional normal phase/reverse phase HPLC-MS/MS protocols. While this approach has the advantage of maximized quantitative aspects, it can also suffer from the potential loss of information/detection, particularly with regard to extremely low abundance species. This explains the identified 146 major PL species rather than thousands of “rear” species in the lipidome of HeLa cells. Among this diversified group, polyunsaturated fatty acid (PUFA)-containing species—potential targets of redox opto-modifications—were represented by 102 molecular species.

### Selective Accumulation of NAO in Mitochondria Is Membrane-Potential-Dependent

Our previous work has demonstrated that early oxidation of mitochondrial CLs is a required stage in the execution of the intrinsic apoptotic program leading to the release of cytochrome c from mitochondria into the cytosol.[13] With this in mind, we tried to find the conditions where a photosensitizer, NAO, would be confined exclusively to mitochondria. We established that in the range of low concentrations of 25, 50, and 100 nM, NAO demonstrated excellent selectivity for mitochondria as indicated by its colocalization with a mitochondria-specific probe, Mitotracker Deep Red, in mouse embryonic cells (MECs; Figure 1a, top panel).[14] Consistently, in HeLa cells, NAO at the concentration of 100 nM also colocalized with Mitotracker Deep Red (Figure 1a, bottom panel). While NAO has been shown to have a high affinity to CL,[11] this occurs under conditions where the concentration of NAO is relatively low and most of the NAO accumulates in the IMM in a membrane potential manner. It should be noted, however, that other potential candidate interacting PLs, PG, PI, and phosphatidylinositolphosphates (PIPs) are present in mitochondria, albeit at lower concentrations, particularly in the inner mitochondrial membrane[15]—the site of NAO localization in functional nondepolarized mitochondria. A higher concentration of NAO (1 $\mu$M) can result in a saturation of the mitochondrial accumulation (Supporting Information Figure S1), and NAO in turn binds to other nonmitochondrial PLs, partially due to hydrophobic and electrostatic interactions.

Because partitioning of NAO into mitochondria is membrane-potential-(MMP) dependent,[16] we endeavored to use a protonophoric uncoupler, FCCP, to assess the specificity of NAO action in mitochondria. Indeed, MMP depolarization in FCCP-treated HeLa cells, indicated by JC-1, a mitochondrial membrane potential probe (Figure 1b), caused a dramatic drop of NAO mean fluorescence intensity (MFI; Figure 1c). To further explore the MMP dependence in NAO's mitochondrial effects, we performed live cell imaging experiments using MMP-dependent and MMP-independent mitochondrial markers—tetramethylrhodamine (TMRM) and a mitochondria-targeted genetically encoded fluorogenic activating protein (mFAP), respectively. In NAO treated cells, the sensitizer colocalized with both mFAP and TMRM, indicating its mitochondrial accumulation (top panel in Figure 1d). By contrast, when cells were pretreated with FCCP followed by NAO staining, both NAO and TMRM dyes diffused into extramitochondrial compartments (bottom panel in Figure 1d). Moreover, when cells were treated with FCCP after NAO staining, TMRM staining in cells significantly decreased (within 15 min) and NAO diffused from mitochondria into other cellular compartments, whereas mFAP, as expected, remained associated with mitochondria.

## NAO Facilitates Opto-Activated Apoptosis in Both CL- and MMP-Dependent Manners

We further tested NAO as a photosensitizer of apoptotic cell death. Very few HeLa cells underwent apoptosis either immediately (0.5 h) or at 6 h following light exposure. By contrast, a significant increase of apoptotic cells was observed at 24 h, and this effect increased over time as evidenced by PS externalization (Figure 2a). The effect was dependent on the light intensity (from 2.9 to 11.4 W/cm$^2$, Figure 2b). The light intensity with an irradiance of 5.7 W/cm$^2$ was selected for the subsequent experiments. The combined effect of NAO plus light was synergistically higher than that of the light alone or NAO alone (Figure 2b). Another common biomarker of apoptosis, elevated caspase activity, was also observed during NAO-photosensitized cell death (Figure 2c).

To confirm the role of CL in apoptosis, we employed HeLa cells with knocked-down CL synthase (CLS) in which selectively lowered CL content (from 20.8 to 9.2 pmol/nmol total PL phosphorus) has been achieved without a difference in the levels of other major PLs (PC, PE, PI, PA) except a >55% increase of PG.[17] Of note, a loss of more than half of the CL content in HeLa cells was not associated with the significant changes of bioenergetics parameters, including measurement of the ATP levels and the mitochondrial membrane potential.[17] These CL-deficient HeLa cells demonstrated increased resistance to NAO-dependent apoptosis upon light exposure (Figure 2d). In similar experiments, we established that NAO facilitated light-induced apoptosis in MEC cells (Supporting Information Figure S2).

Protonophoric uncouplers, such as FCCP, have been previously used to induce either mitophagy or apoptosis through depolarization of the mitochondria. In contrast, FCCP induced depolarization prevented specific accumulation of NAO in the inner leaflet of the inner mitochondrial membrane facing the matrix and suppressed photoinduced CL oxidation. As CL oxidation is a required mitochondrial step in the execution of the apoptotic program, FCCP protected cells against photoinduced NAO-mediated apoptosis. This was

documented by FCCP-dependent suppression of (i) PS externalization (Figure 3a), (ii) DNA fragmentation from TUNEL assay (Figure 3b), and (iii) caspase activation (Figure 3c). We were encouraged to use this protective effect of FCCP in a redox opto-lipidomics search for cell death signals.

## Redox Opto-Lipidomics Detects Pro-Apoptotic Signals

Accumulation of irreparable damage, commonly DNA damage, triggers p53-mediated signaling cascades realized in the execution of an intrinsic apoptotic cell death program which includes CL oxidation.[18] We reasoned that direct NAO-photosensitized CL oxidation may be associated with the immediate generation of lipid apoptotic death signals. Therefore, we employed the redox opto-lipidomics approach to reveal oxidatively modified PLs, particularly CLs, immediately following light exposure. Specifically, we performed a targeted lipidomics search for newly emerged oxygenated derivatives of PLs in NAO treated cells and established a high selectivity of light-evoked redox modifications of lipids. Out of 102 total molecular species of PUFA−PLs amenable to oxidation, there were 13 oxygenated CLs, 21 oxygenated PEs, 22 oxygenated PCs, and two oxygenated PSs, whose levels increased to different extents immediately after illumination (Supporting Information Table S1). However, among all the oxygenated PLs, only the total levels of oxygenated CLs and PCs significantly increased (>6-fold) immediately following NAO induced light reaction (Figure 4a). Surprisingly, there was a 61-fold increase of mono-oxygenated CLs but no change of dioxygenated CLs immediately following light reaction, whereas both mono- and dioxygenated PCs responded similarly with only a 6.3-fold increase (Figure 4b). Thus, mono-oxygenation of CLs was markedly more selective during the NAO induced light reaction. Moreover, mono-oxygenated CLs with C18:2 demonstrated a more robust increase than those with C20:4 (47-fold vs 14-fold increase) immediately following NAO induced light reaction (Figure 4c). The maximal formation of oxygenated CLs was detected right after the 30 min of light exposure and gradually declined in the course of the dark incubation (Figure 4a, b, and c).

With regard to mechanisms of the loss of oxidized CL species in the course of dark incubation, we hypothesized that hydrolysis of the oxidation products might have taken place. $Ca^{2+}$-independent phospholipases $A_2$ have been identified as potent catalysts of hydrolysis of peroxidized CLs.[19] To test this hypothesis, we performed normal phase LC-MS/MS analysis of monolyso-CLs (MLCLs), one of the products of the hydrolytic reaction.[20] We identified eight major species of MLCLs based on high accuracy $m/z$ values and corresponding MS/MS fragments (Supporting Information Figure S3). The quantitative data showed that the total amount of MLCLs was more than 4-fold higher in the cells exposed to light in the presence of NAO and subsequently incubated in the dark for 48 h compared to NAO + Light (the 0.5 h group). The increased levels of MLCLs were not observed in the cells pretreated with FCCP, then exposed to light in the presence of NAO and incubated for 48 h in the dark. Our data indicate that hydrolysis of oxygenated CLs generated during NAO-photosensitized oxidation might be responsible, at least in part, for the decay of CL peroxidation products. For example, MLCL(18:1/18:2/ 18:1) ($m/z$ 1189.7658), MLCL(18:1/18:1/18:1) ($m/z$ 1191.7769), MLCL(18:1/20:4/18:2) ($m/z$ 1213.7657), and MLCL(18:1/18:2/18:2) ($m/z$ 1187.7506) might be partially generated from

the decay of CL(18:1/18:2/18:1/18:2+[O]) ($m/z$ 1467.9906), CL(18:1/18:1/18:1/18:2+[O]) ($m/z$ 1469.9979), CL(18:1/20:4/18:2/18:2+[O]) ($m/z$ 1491.9906), and CL(18:1/18:2/18:2/18:2+[O]) ($m/z$ 1465.9749), respectively.

To establish the association of the light induced lipid signals with the execution of the apoptotic program, we tested the effect of FCCP–which protected against NAO photosensitized apoptosis—on lipid oxidation. The only oxygenated lipid products suppressed both immediately and at 48 h following light exposure by FCCP were mono-oxygenated C18:2-containing CL species (Figure 4c). Shown in Figure 4d are the representative mass spectra of nonoxygenated CLs from control (in black) and mono-oxygenated CLs with C18:2 generated from NAO-loaded cells immediately following light exposure (in red). A representative MS/MS spectrum of mono-oxygenated CL (CL(18:1/18:2+[O]/18:2/18:1), $[M-H]^-$, $m/z$: 1467.9906) is demonstrated in Figure 4e.

We chose to reconfirm the possible function of C18:2-contaning oxygenated CL species as death signals by comparing them with the CL lipid oxidation products profiles of HeLa cells triggered to apoptosis by a prototypical agent, actinomycin D, previously reported to cause CL oxidation.[13] Notably, these same oxygenated CL species we detected in light reaction were also identified in actinomycin D-induced apoptosis (Supporting Information Figure S4).

## Bioinformatics Analysis of Pro-Apoptotic Oxygenated Lipid Signals in CLs

To help visualize and facilitate a more intuitive analysis of complex optolipidomics results, we developed a bioinformatics pipeline consisting of Venn diagrams and n-gram analysis commonly used in language analysis.

Venn diagrams were created to enable comparison of light with other previously studied apoptotic conditions as they allow highlighting the intersection of lipid oxidation product profiles in the presence of the different apoptosis inducing agents. The Venn diagram in Figure 5a compares the CL lipid oxidation product profiles obtained here in response to light to CL oxidation products detected during apoptosis triggered by conventional agents, such as actinomycin D,[13] staurosporine,[13] and ionizing radiation.[21,22] By comparing the NAO + light triggered apoptosis in HeLa cells with the effects of three different cell death inducers in mouse embryonic cells and *in vivo* in mouse lung tissue, we confirmed the universal correlation of mono-oxygenated C18:2 CL species with the execution of an apoptotic program in mitochondria (Figure 5a).

N-gram analysis is a term borrowed from statistical language modeling of the co-occurrence of words, where N refers to the number of words (e.g., the bigram “New York”, N = 2). It has previously been applied to biology using aminio acids or nucleotides as the word equivalents.[23,24] Here, we extended the approach to consider the lipid acyl chain as a novel word equivalent (see Methods). N-gram analysis provides an intuitive way to compare the frequencies and specificity of opto-lipidomic pro-apoptotic response with those triggered by other inducers of cell death. Assuming that one of the four acyls of CL designates a word in the signaling language, we found that C18:2 mono-oxygenated CLox species had the highest frequency in unigram analysis (Figure 5b). This high participation of C18:2ox-containing

CL species was also observed in other pro-apoptotic stimuli (Figure 5b). Different n-grams (combinations of different CL acyls) in bi-, tri-, and tetra-gram frequency plots also showed the same trend for oxygenated C18:2-containing CL species, but in these cases the signal was spread across different grams (Supporting Information Figures S5–S8). Notably, NAO +light specifically induced apoptosis, while other stimuli (several *in vitro* and *in vivo* treatments and exposures of cells and animals denoted in the legends of Figure 5 and Supporting Information Figures S5–S8) can trigger apoptosis along with alternative death pathways (Figure 5b). Comparing the LC-MS results of NAO +light triggered apoptosis with previously obtained data where other pro-apoptotic stimuli were used, we found that mono- and dioxygenated C18:2-containing CL species were specific for the current experiments ($\chi$-squared test, $p < 0.05$, Supporting Information Table S2), thus suggesting that these signals are specific and correlated with the execution of apoptosis.

Here, we report, for the first time, a redox opto-lipidomics approach based on a combination of high affinity light-sensitive ligands to specifically localized PLs using an LC-MS based redox lipidomics analysis and a novel lipid n-gram bioinformatics pipeline which was applied to the characterization of lipid cell death signals during the execution of an intrinsic apoptotic program in mitochondria. We identified mono-oxygenated derivatives of C18:2-containing CLs as oxidation products formed in mitochondria after the exposure of NAO-loaded cells to light. We ascertained that these signals emerge as immediate opto-lipidomics responses and are similar to those previously described among CL oxidation products detected during apoptosis triggered by conventional agents, such as actinomycin D,[13] staurosporine,[13] and ionizing radiation.[21,22] We further established that the function(s) of these products is realized right after the light exposure, and they decay long before the commencement of apoptotic cell death. By depolarizing the MMP[18,19] and preventing mitochondrial NAO accumulation, FCCP—known to cause injury—blocked the formation of characteristic derivatives of oxygenated C18:2-CL products and protected cells from photosensitized apoptotic death.

The success of redox opto-lipidomics depends, to a large extent, on the selectivity of the photosensitizing ligand toward particular types of lipids. In this regard, CLs offer a particular advantage as this mitochondria-unique PL is localized almost exclusively to the IMM.[25] Thus, a combination of MMP-dependent delivery to the mitochondrial matrix with a high affinity for CLs[11] made NAO an exceptionally CL-selective opto-lipidomics sensitizer. NAO's selectivity toward CL was further enhanced by the lack from the mitochondria of another anionic NAO target—PS, which is effectively decarboxylated to PE.[26] A small but significant amount of PC also underwent NAO-dependent oxidation. These oxidized PCs were insensitive to mitochondrial depolarization by FCCP, indicating that NAO might also bind to PCs in extra-mitochondrial compartments, possibly in close proximity to other anionic PLs. However, the role of PCs in apoptotic signaling, if any, was minimal as they were not detected by redox lipidomic analysis in cells undergoing apoptosis triggered by other reagents.[13] Notably, PC and PE mono-oxygenated species have been recently identified as potential death signals in nonapoptotic pathways of cells during ferroptosis associated with Gpx4-deficiency.[27]

In addition to selectivity of interactions with a particular PL, chemical propensities of photosensitizers along with the rates of metabolic conversions of oxygenated PLs may be important for redox opto-lipidomics analysis. Photosensitized oxidation of lipids can proceed via type I or type II mechanisms.[28] The former involves free radicals such as those formed by triplet sensitizer-reducing substrate interactions, whereas the latter typically involves singlet oxygen ($^1O_2$) formed by triplet sensitizer-ground state oxygen interactions.[29] It is believed that light-induced intracellular effects of acridines are predominantly realized via the production of singlet oxygen.[30] Therefore, we performed experiments in which we investigated the effects of two singlet oxygen quenchers (lycopene and beta-carotene)[31] on light induced apoptosis. We found that both of them exerted significant protection against light induced apoptosis in the presence of NAO (Supporting Information Figure S9), suggesting that the singlet oxygen-driven reactions are significant contributors to CL oxidation and apoptosis. Notably, the inhibitors did not cause 100% protection against light induced NAO-mediated apoptosis. This suggests that alternative, likely type I, mechanisms can also contribute to CL photo-oxidation in the presence of NAO. Indeed, vitamin E—known to act as both a singlet oxygen quencher and free radical scavenger—was more effective in protecting against light induced cell death in the presence of NAO than lycopene and beta-carotene (54%, 31%, and 34% protection by vitamin E, lycopene, and $\beta$-carotene, respectively). While these data suggest that singlet oxygen mediated effects were important contributors to cell death, they also indicate that alternative, likely type I driven, mechanisms of photosensitization were involved. Quantitatively, this can be addressed by detailed analysis of CL oxidation products by LC-MS/MS fragmentation analysis of oxygenated fatty acid residues. Indeed, singlet oxygen attack on linoleoyl-containing CLs will generate 10-OOH and 12-OOH nonconjugated products, whereas free radical attack will yield 9-OOH and 13-OOH isomers.[32] While these measurements are technically feasible, they require large amounts of cell/lipids for analysis because of the low abundance of the CL oxidation products and represent the subject of future studies.

Both photosensitized free radical mechanisms and singlet oxygen-driven reactions should yield dioxygenated PL species.[33] However, only a minor presence of these products has been detected after NAO-sensitized oxidation of CLs, suggesting the involvement of effective cellular reduction mechanisms.[34] This reduction may be enzymatically catalyzed by a well-known thiol-dependent mechanism (e.g., glutathione peroxidase 4, Gpx4) or via heme-peroxidase reactions (e.g., cytochrome C/CL complexes). As an illustration of the Gpx4-dependent pathway, we found effective TLCL-OOH reduction by Gpx4 present in homogenates of naïve HeLa cells but not in the homogenates of cells pretreated with a specific Gpx4 inhibitor, RSL3[35] (Supporting Information Figure S12). To demonstrate the effectiveness of the cytochrome c-catalyzed reaction, we performed *in vitro* experiments and showed that cytochrome c can effectively reduce tetra-linoleoyl-hydroperoxy CL (TLCL-OOH) to tetra-linoleyl hydroxy-CL (TLCL−OH; Supporting Information Figure S11).

Many PL class-specific organelle-targeted fluorescent probes have been recently developed[36] with a potential of being used for redox opto-lipidomics. Among those are recently reported improved fluorescent probes for CL.[37] Recently, a powerful approach based on the employment of caged lipids, membrane-permeable photoactivatable derivatives

of different PLs has been developed to specifically probe signaling pathways at the single cell level.[3839,40] Caged lipids are designed to contain a photocleavable group attached to a position that is crucial for their function, thus rendering lipid analogs inactive. Light induced cleavage of the protective group liberates the active lipid to achieve its necessary intracellular concentration. While a variety of caged lipid analogs have been synthesized in several major classes (PA, PIs, PEs, sphingolipids, ceramides and ceramide 1-phosphate, triacylglycerols),[38,41] no caged CLs have been reported so far. It is tempting to speculate that caged CLs and CLox could be instrumental to the identification of the mechanisms through which they facilitate the execution of apoptotic cell death. One can also assume that caged CL analogs may be designed with a potential to photosensitize CL oxidation.

Even though the reason why mono-oxygenated CLs significantly decrease at 48 h following treatment is still elusive, we speculate that certain phospholipase (e.g., Cld1) in cells might be responsible for eliminating these potential death signals, which explains the formation of MLCL after a period of time (Supporting Information Figure S3). Our previous work has identified CL oxidation as a required stage of execution of the mitochondrial stage of the intrinsic apoptotic program triggered by a number of toxic agents such as actinomycin D, staurosporine, 6-hydroxydopamine, etc.[13,42] In these cases, oxidative catalysis occurred within complexes of CL with cytochrome c (cyt c) acting as a peroxidase[13] whereby CL oxidation products were necessary for the release of cyt c from mitochondria into the cytosol and its subsequent role in the formation of apoptosomes, activation of caspases, and subsequent proteolytic events culminating in the completion of the apoptotic program.[43,44] The exact proximate mechanisms of CL oxidation products in facilitating the release of cyt c remain enigmatic, although candidate pathways may include their interactions with pro-apoptotic proteins, Bax/Bak, in the outer mitochondrial membrane.[45] The series of pro-apoptotic processes that include translocation of the required cytosolic proteins into the outer mitochondrial membrane (Bax/Bak) and *vice versa* from mitochondria into the cytosol (cyt c) initiated by CL oxidation products proceed over a period of 9–24 h.[13,46] In line with this, we observed a significant increase of cell death (~20%) at 24 h and its further enhancement (34%) at 48 h following NAO photosensitization. We believe that NAO-mediated light-driven CL oxidation triggered similar pro-apoptotic processes whose development over time caused typical manifestations of apoptotic cell death such as DNA fragmentation, caspase 3/7 activation, and PS externalization.

NAO applications in redox opto-lipidomics may also be useful for the identification of critical targets for cancer phototherapy. Indeed, the well documented propensity of cancer cells to repair DNA from damaging effects of radiation and cytotoxic drugs is of major significance in their profound resistance to radiation and chemotherapy.[47] This resulted in attempts to explore photosensitizing molecules capable of inducing mitochondria-mediated apoptosis as a potentially effective alternative approach.[47] Among several mitochondria-targeted photodynamic therapy reagents,[48,49] phthalocyanines (e.g., Pc4) were reportedly localized in the proximity of CLs.[50] The identification of NAO induced CL oxidation products correlating with the execution of apoptotic cell death signals may serve as an important guide in optimizing the efforts in successful photodynamic therapy of cancer.

Overall, our results extend the remarkable achievements and power of opto-genetics in studies of macromolecule-driven intracellular pathways to the field of small PL molecules resilient to opto-genetic manipulations.

## METHODS

This section describes key experiments only; an extended experimental section is provided in the Supporting Information.

### Irradiation Treatments

Cells were incubated with 100 nM NAO for 30 min in whole medium (DMEM-15% FBS) and washed with medium before exposure to light. Irradiations were performed by using an ARC lamp device (Oriel Instruments) with a 435 nm long pass color filter (Thorlabs Inc.). The irradiance of 5.7 W/cm$^2$ was used in most experiments except those employed in the experiment (Figure 2a) for the optimization of irradiance conditions where light intensities range from 2.9 to 11.4 W/cm$^2$.

### Microscopic Imaging of NAO and Mitochondria

Cells were seeded in 35 mm glass-bottomed tissue culture dishes (MatTek Corp.) prior to infection with an adenoviral vector expressing mitochondrially targeted fluorogen activating protein (mFAP).[51] At 48 h following transfection, cells were pretreated with NAO (25, 50, or 100 nM) and 200 nM tetramethylrhodamine (TMRM) or 200 nM MitoTracker Deep Red (M-22426; Invitrogen) for 30 min. Malachite green (5 nM) was added at 15 min prior to imaging to reveal the mFAP transgene (thereby defining the mitochondria[52]). Cells were washed with medium before imaging. All images were acquired using a Nikon Ti inverted microscope (Nikon Inc.) using NIS-Elements Software (Nikon Inc.) and a 60× 1.49NA oil optic and equipped with a SpectraX diode based light source (Lumencor), Chroma Technology Inc. filer sets, and an ORCA-Flash4.0 V2 digital cMOS camera (Hamamatsu).

### Analysis of PLs and Their Oxygenated Molecular Species by SPE-2D-LC-MS

The analysis flowchart is shown in Supporting Information Figure S10. Lipids were extracted using the Folch procedure and redissolved in 250 μL of chloroform/methanol (2:1; v/v).[53] Lipid phosphorus was measured by phosphorus measurement using a micro-method.[54] A certain amount of lipid extract corresponding to 3 μg of phosphorus, which was spiked with internal standards, was dried under nitrogen, and reconstituted in 0.5 mL of hexane/chloroform/methanol (95:3:2; v/v/v). The following solid phase extraction (SPE) was conducted as previously described with slight modification.[55] The SPE protocol is described in detail in the Supporting Information. Each fraction from SPE was further injected into the normal phase high performance liquid chromatograph (HPLC) on a Luna silica column (2.0 mm × 15 cm, 3 μm, Phenomenex) as the first dimension. The condition of LC-MS/MS was optiomized by injecting chemical standard of tetra-linoleyl CL. The LC-MS/MS method was provided in detail in the Supporting Information. Additionally, the LC-MS/MS method for measuring MLCL was also provided in the Supporting Information.

## Lipid Identification and Analysis

Data files from the control samples were analyzed by SimLipid 4.30 (PREMIER Biosoft). Each nonoxygenated PL except CL was identified by matching its corresponding MS/MS spectrum. Nonoxygenated CLs were identified manually by Xcalibur Qual (Thermo Scientific). Based on all the PLs identified, possible oxygenated species were projected, including plus one and two oxygen atoms. Each lipid was further quantified by Xcalibur Quan (Thermo Scientific) based on its accurate $m/z$ value with an accuracy of 5 ppm.

## Bioinformatics

A four-way Venn diagram analysis was applied to the lists of oxygenated CL species identified from the current study and three other studies. The Venn diagram was plotted using VENNY 2.0 (http://bioinfogp.cnb.csic.es/tools/venny/).

N-gram analysis (specifically uni-, bi-, tri-, and tetra-gram analysis) was carried out using the lists of oxygenated CL species from the current study and the other previous ones[19,21,22,56–63] using the text2wngram program from the CMU-Cambridge Statistical Language Modeling Toolkit v2 (http://svr-www.eng.cam.ac.uk/~prc14/toolkit.html). This tool computes the frequencies of single words (unigrams), pairs of correlative words (bigrams), and in general, the frequencies of groups of N correlative words (N-grams) in a text. To analyze the frequencies of different species of oxygenated CL with this tool, we need to transform the structural information on CL molecules into word-like units. To this end, we assumed that each of the four acyls of CL designates a word in the lipid signaling language, and that each CL molecule designated a complete meaningful sentence. Hence, to compute different grams we first coded the different types of acyl chains in CL molecules as L:P–O where L represents the length of the chain, P the unsaturated position in the chain, and O the oxygen containing substituent in such an unsaturated position (as represented elsewere in the present work). Then, we computed unigrams on that set of coded CL acyl chains (this is frequencies of each of the coded CL acyl chains). To compute bi-, tri-, and tetra-grams, only combinations of two, three, and four correlative coded acyl chains within the CL molecule were considered, respectively. To be consistent with the assumed model where each CL molecule designated a complete meaningful sentence, we did not allow for the analysis of N-grams consisting of acyl chains of more than one CL molecule.

Results from previous studies were grouped into two different categories *in vitro* and *in vivo* according to the nature of each of the referred to experiments in order to provide an easier comparison to the previous study. We assessed the statistical significance of differences between frequencies of unigrams observed in the current work and frequencies of such unigrams in previous studies (grouped in *in vivo* and *in vitro* categories) using $\chi$-squared tests. Frequencies of all N-grams and the $\chi$-squared test were computed using R.[64]

## Statistical Analysis

The data are presented as mean ± standard deviation (SD) values from three replicates. Heat maps of fold change were generated by Microsoft Office Excel 2013 to visualize the trend and identify the death signals. Statistical analysis was performed using either an unpaired Student's *t*-test or the one-way analysis of variance with Tukey's postanalysis. Homogeneity

of variance was assumed with a 95% confidence interval level. Results from at least $n = 3$ with $p < 0.05$ were considered significant. All statistical analyses were performed using SPSS software Standard version 18.0 (SPSS Inc.).

## Supplementary Material

Refer to Web version on PubMed Central for supplementary material.

## Acknowledgments

This work was supported by the National Institutes of Health (EB17268, ES020693, U19AIO68021, HL114453, NS076511, NS061817, NS052315, CA 165065), the National Institute for Occupational Safety and Health (OH008282), the National Center for Research Resources (S10RR023461), Human Frontier Science Program (HFSP-RGP0013/2014), and the Barth Syndrome Foundation, Inc. and the Barth Syndrome Foundation of Canada. We are grateful to M. Bruchez (Carnegie Mellon University) for providing dyes and reagents associated with the FAP technology, and M. Larsson of the Center for Biologic Imaging at the University of Pittsburgh for generation of adenoviral FAP constructs.

## LIST OF ABBREVIATIONS

| | |
|---|---|
| **CL** | cardiolipin |
| **CLS** | cardiolipin synthase |
| **DMEM** | Dulbecco's Modified Eagle's Medium |
| **FBS** | fetal bovine serum |
| **FCCP** | carbonyl cyanide p-trifluoromethoxyphenyl hydrazine |
| **HPLC** | high performance liquid chromatography |
| **IMM** | inner mitochondrial membrane |
| **JC-1** | 5,5′,6,6′-tetrachloro1,1′,3,3′-tetraethylbenzimidazolyl carbocyanine iodide |
| **MEC** | mouse embryonic cell |
| **MMP** | mitochondrial membrane potential |
| **NAO** | 10-nonylacridine orange bromide |
| **OMM** | outer mitochondrial membrane |
| **PC** | phosphatidylcholine |
| **PE** | phosphatidylethanolamine |
| **PG** | phosphatidylglycerol |
| **PI** | phosphatidylinositol |
| **PIP** | phosphatidylinositol phosphate |
| **PL** | phospholipid |

| | |
|---|---|
| **PS** | phosphatidylserine |
| **PUFA** | polyunsaturated fatty acid |
| **SPE** | solid phase extraction |
| **TMRM** | tetramethylrhodamine |

## References


1. Toettcher JE, Voigt CA, Weiner OD, Lim WA. The promise of optogenetics in cell biology: interrogating molecular circuits in space and time. Nat Methods. 2011; 8:35–38. [PubMed: 21191370]
2. Welberg L. Techniques: Optogenetics takes more control. Nat Rev Neurosci. 2013; 14:587. [PubMed: 23942468]
3. Wu Y, Li SS, Jin X, Cui N, Zhang S, Jiang C. Optogenetic approach for functional assays of the cardiovascular system by light activation of the vascular smooth muscle. Vasc Pharmacol. 2015; 71:192.
4. Kim KH. The rise of on-demand research and specific applications: optogenetics in urology. Int Neurourol J. 2015; 19:1–2. [PubMed: 25833474]
5. Henriksen BS, Marc RE, Bernstein PS. Optogenetics for retinal disorders. J Ophthalmic Vis Res. 2014; 9:374–382. [PubMed: 25667740]
6. Xia Y, Sengupta K, Maggiani A, Qu F, Peng L. A bola-phospholipid bearing tetrafluorophenylazido chromophore as a promising lipid probe for biomembrane photolabeling studies. Org Biomol Chem. 2013; 11:5000–5005. [PubMed: 23783551]
7. Giraldo AMV, Castello PR, Flecha FLG, Moeller JV, Delfino JM, Rossi JP. Stoichiometry of lipid-protein interaction assessed by hydrophobic photolabeling. FEBS Lett. 2006; 580:607–612. [PubMed: 16412439]
8. Schlame M, Haldar D. Cardiolipin is synthesized on the matrix side of the inner membrane in rat liver mitochondria. J Biol Chem. 1993; 268:74–79. [PubMed: 8380172]
9. Schlame M, Brody S, Hostetler KY. Mitochondrial cardiolipin in diverse eukaryotes. Comparison of biosynthetic reactions and molecular acyl species. Eur J Biochem. 1993; 212:727–735. [PubMed: 8385010]
10. Jiang F, Ryan MT, Schlame M, Zhao M, Gu Z, Klingenberg M, Pfanner N, Greenberg ML. Absence of cardiolipin in the crd1 null mutant results in decreased mitochondrial membrane potential and reduced mitochondrial function. J Biol Chem. 2000; 275:22387–22394. [PubMed: 10777514]
11. Petit JM, Maftah A, Ratinaud MH, Julien R. 10N-nonyl acridine orange interacts with cardiolipin and allows the quantification of this phospholipid in isolated mitochondria. Eur J Biochem. 1992; 209:267–273. [PubMed: 1396703]
12. Mileykovskaya E, Dowhan W, Birke RL, Zheng D, Lutterodt L, Haines TH. Cardiolipin binds nonyl acridine orange by aggregating the dye at exposed hydrophobic domains on bilayer surfaces. FEBS Lett. 2001; 507:187–190. [PubMed: 11684095]
13. Kagan VE, Tyurin VA, Jiang J, Tyurina YY, Ritov VB, Amoscato AA, Osipov AN, Belikova NA, Kapralov AA, Kini V, Vlasova II, Zhao Q, Zou M, Di P, Svistunenko DA, Kurnikov IV, Borisenko GG. Cytochrome c acts as a cardiolipin oxygenase required for release of proapoptotic factors. Nat Chem Biol. 2005; 1:223–232. [PubMed: 16408039]
14. Rodriguez ME, Azizuddin K, Zhang P, Chiu SM, Lam M, Kenney ME, Burda C, Oleinick NL. Targeting of mitochondria by 10-N-alkyl acridine orange analogues: role of alkyl chain length in determining cellular uptake and localization. Mitochondrion. 2008; 8:237–246. [PubMed: 18514589]
15. de Kroon AI, Dolis D, Mayer A, Lill R, de Kruijff B. Phospholipid composition of highly purified mitochondrial outer membranes of rat liver and Neurospora crassa. Is cardiolipin present in the mitochondrial outer membrane? Biochim Biophys Acta, Biomembr. 1997; 1325:108–116.

16. Jacobson J, Duchen MR, Heales SJ. Intracellular distribution of the fluorescent dye nonyl acridine orange responds to the mitochondrial membrane potential: implications for assays of cardiolipin and mitochondrial mass. J Neurochem. 2002; 82:224–233. [PubMed: 12124423]
17. Huang Z, Jiang J, Tyurin VA, Zhao Q, Mnuskin A, Ren J, Belikova NA, Feng W, Kurnikov IV, Kagan VE. Cardiolipin deficiency leads to decreased cardiolipin peroxidation and increased resistance of cells to apoptosis. Free Radical Biol Med. 2008; 44:1935–1944. [PubMed: 18375209]
18. Hoye AT, Davoren JE, Wipf P, Fink MP, Kagan VE. Targeting mitochondria. Acc Chem Res. 2008; 41:87–97. [PubMed: 18193822]
19. Tyurina YY, Poloyac SM, Tyurin VA, Kapralov AA, Jiang J, Anthonymuthu TS, Kapralova VI, Vikulina AS, Jung MY, Epperly MW, Mohammadyani D, Klein-Seetharaman J, Jackson TC, Kochanek PM, Pitt BR, Greenberger JS, Vladimirov YA, Bayir H, Kagan VE. A mitochondrial pathway for biosynthesis of lipid mediators. Nat Chem. 2014; 6:542–552. [PubMed: 24848241]
20. Ma BJ, Taylor WA, Dolinsky VW, Hatch GM. Acylation of monolysocardiolipin in rat heart. J Lipid Res. 1999; 40:1837–1845. [PubMed: 10508203]
21. Tyurina YY, Tyurin VA, Epperly MW, Greenberger JS, Kagan VE. Oxidative lipidomics of gamma-irradiation-induced intestinal injury. Free Radical Biol Med. 2008; 44:299–314. [PubMed: 18215738]
22. Tyurina YY, Tyurin VA, Kapralova VI, Wasserloos K, Mosher M, Epperly MW, Greenberger JS, Pitt BR, Kagan VE. Oxidative lipidomics of gamma-radiation-induced lung injury: mass spectrometric characterization of cardiolipin and phosphatidylserine peroxidation. Radiat Res. 2011; 175:610–621. [PubMed: 21338246]
23. Ganapathiraju M, Manoharan V, Klein-Seetharaman J. BLMT: statistical sequence analysis using N-grams. Appl Bioinf. 2004; 3:193–200.
24. Ganapathiraju, M., Balakrishnan, N., Reddy, R., Klein-Seetharaman, J. Ambient Intelligence for Scientific Discovery, Lecture Notes in Computer Science. Springer; Berlin: 2005. Computational Biology and Language.
25. Cheneval D, Muller M, Toni R, Ruetz S, Carafoli E. Adriamycin as a probe for the transversal distribution of cardiolipin in the inner mitochondrial membrane. J Biol Chem. 1985; 260:13003–13007. [PubMed: 4055730]
26. Dygas A, Zborowski J, Wojtczak L. Decarboxylation of phosphatidylserine by rat liver mitochondria. Acta Biochim Pol. 1980; 27:153–161. [PubMed: 7435081]
27. Friedmann Angeli JP, Schneider M, Proneth B, Tyurina YY, Tyurin VA, Hammond VJ, Herbach N, Aichler M, Walch A, Eggenhofer E, Basavarajappa D, Radmark O, Kobayashi S, Seibt T, Beck H, Neff F, Esposito I, Wanke R, Forster H, Yefremova O, Heinrichmeyer M, Bornkamm GW, Geissler EK, Thomas SB, Stockwell BR, O'Donnell VB, Kagan VE, Schick JA, Conrad M. Inactivation of the ferroptosis regulator Gpx4 triggers acute renal failure in mice. Nat Cell Biol. 2014; 16:1180–1191. [PubMed: 25402683]
28. Foote CS. Mechanisms of photosensitized oxidation. There are several different types of photosensitized oxidation which may be important in biological systems. Science. 1968; 162:963–970. [PubMed: 4972417]
29. Girotti AW. Photosensitized oxidation of membrane lipids: reaction pathways, cytotoxic effects, and cytoprotective mechanisms. J Photochem Photobiol. 2001; B63:103–113.
30. Zdolsek JM. Acridine orange-mediated photodamage to cultured cells. APMIS. 1993; 101:127–132. [PubMed: 8387800]
31. Di Mascio P, Devasagayam TP, Kaiser S, Sies H. Carotenoids, tocopherols and thiols as biological singlet molecular oxygen quenchers. Biochem Soc Trans. 1990; 18:1054–1056. [PubMed: 2088803]
32. Frankel EN. Chemistry of free radical and singlet oxidation of lipids. Prog Lipid Res. 1984; 23:197–221. [PubMed: 6100997]
33. Dolmans DE, Fukumura D, Jain RK. Photodynamic therapy for cancer. Nat Rev Cancer. 2003; 3:380–387. [PubMed: 12724736]
34. Winterbourn CC. The biological chemistry of hydrogen peroxide. Methods Enzymol. 2013; 528:3–25. [PubMed: 23849856]

35. Dixon SJ, Lemberg KM, Lamprecht MR, Skouta R, Zaitsev EM, Gleason CE, Patel DN, Bauer AJ, Cantley AM, Yang WS, Morrison B 3rd, Stockwell BR. Ferroptosis: an iron-dependent form of nonapoptotic cell death. Cell. 2012; 149:1060–1072. [PubMed: 22632970]
36. Shioji K, Oyama Y, Okuma K, Nakagawa H. Synthesis and properties of fluorescence probe for detection of peroxides in mitochondria. Bioorg Med Chem Lett. 2010; 20:3911–3915. [PubMed: 20605449]
37. Leung CW, Hong Y, Hanske J, Zhao E, Chen S, Pletneva EV, Tang BZ. Superior fluorescent probe for detection of cardiolipin. Anal Chem. 2014; 86:1263–1268. [PubMed: 24372165]
38. Höglinger D, Nadler A, Schultz C. Caged lipids as tools for investigating cellular signaling. Biochim Biophys Acta, Mol Cell Biol Lipids. 2014; 1841:1085–1096.
39. Feng S, Laketa V, Stein F, Rutkowska A, MacNamara A, Depner S, Klingmüller U, Saez-Rodriguez J, Schultz C. A Rapidly Reversible Chemical Dimerizer System to Study Lipid Signaling in Living Cells. Angew Chem, Int Ed. 2014; 53:6720–6723.
40. Schultz C, Neef AB, Gadella TW Jr, Goedhart J. Imaging lipids in living cells. Cold Spring Harb Protoc. 2010; 2010 pdb top83.
41. Gomez-Munoz A, Gangoiti P, Rivera IG, Presa N, Gomez-Larrauri A, Ordonez M. Caged ceramide 1-phosphate (C1P) analogs: Novel tools for studying C1P biology. Chem Phys Lipids. 2015; doi: 10.1016/j.chemphyslip.2015.07.019
42. Tyurina YY, Kapralov AA, Jiang J, Borisenko GG, Potapovich AI, Sorokin A, Kochanek PM, Graham SH, Schor NF, Kagan VE. Oxidation and cytotoxicity of 6-OHDA are mediated by reactive intermediates of COX-2 overexpressed in PC12 cells. Brain Res. 2006; 1093:71–82. [PubMed: 16712820]
43. Hao Z, Duncan GS, Chang CC, Elia A, Fang M, Wakeham A, Okada H, Calzascia T, Jang Y, You-Ten A, Yeh WC, Ohashi P, Wang X, Mak TW. Specific ablation of the apoptotic functions of cytochrome C reveals a differential requirement for cytochrome C and Apaf-1 in apoptosis. Cell. 2005; 121:579–591. [PubMed: 15907471]
44. Marsden VS, O'Connor L, O'Reilly LA, Silke J, Metcalf D, Ekert PG, Huang DC, Cecconi F, Kuida K, Tomaselli KJ, Roy S, Nicholson DW, Vaux DL, Bouillet P, Adams JM, Strasser A. Apoptosis initiated by Bcl-2-regulated caspase activation independently of the cytochrome c/Apaf-1/caspase-9 apoptosome. Nature. 2002; 419:634–637. [PubMed: 12374983]
45. Jiang J, Huang Z, Zhao Q, Feng W, Belikova NA, Kagan VE. Interplay between bax, reactive oxygen species production, and cardiolipin oxidation during apoptosis. Biochem Biophys Res Commun. 2008; 368:145–150. [PubMed: 18211809]
46. Finucane DM, Bossy-Wetzel E, Waterhouse NJ, Cotter TG, Green DR. Bax-induced caspase activation and apoptosis via cytochrome c release from mitochondria is inhibitable by Bcl-xL. J Biol Chem. 1999; 274:2225–2233. [PubMed: 9890985]
47. Pilkington GJ, Parker K, Murray SA. Approaches to mitochondrially mediated cancer therapy. Semin Cancer Biol. 2008; 18:226–235. [PubMed: 18203619]
48. Morgan J, Oseroff AR. Mitochondria-based photodynamic anti-cancer therapy. Adv Drug Delivery Rev. 2001; 49:71–86.
49. Kessel D, Luo Y. Mitochondrial photodamage and PDT-induced apoptosis. J Photochem Photobiol. 1998; B42:89–95.
50. Morris RL, Azizuddin K, Lam M, Berlin J, Nieminen AL, Kenney ME, Samia AC, Burda C, Oleinick NL. Fluorescence resonance energy transfer reveals a binding site of a photosensitizer for photodynamic therapy. Cancer Res. 2003; 63:5194–5197. [PubMed: 14500343]
51. Telmer CA, Verma R, Teng H, Andreko S, Law L, Bruchez MP. Rapid, specific, no-wash, far-red fluorogen activation in subcellular compartments by targeted fluorogen activating proteins. ACS Chem Biol. 2015; 10:1239–1246. [PubMed: 25650487]
52. Szent-Gyorgyi C, Schmidt BF, Creeger Y, Fisher GW, Zakel KL, Adler S, Fitzpatrick JA, Woolford CA, Yan Q, Vasilev KV, Berget PB, Bruchez MP, Jarvik JW, Waggoner A. Fluorogen-activating single-chain antibodies for imaging cell surface proteins. Nat Biotechnol. 2008; 26:235–240. [PubMed: 18157118]
53. Folch J, Lees M, Sloane Stanley GH. A simple method for the isolation and purification of total lipides from animal tissues. J Biol Chem. 1957; 226:497–509. [PubMed: 13428781]

54. Böttcher C, Pries C. A rapid and sensitive sub-micro phosphorus determination. Anal Chim Acta. 1961; 24:203–204.
55. Fauland A, Trotzmuller M, Eberl A, Afiuni-Zadeh S, Kofeler H, Guo X, Lankmayr E. An improved SPE method for fractionation and identification of phospholipids. J Sep Sci. 2013; 36:744–751. [PubMed: 23349108]
56. Tyurina YY, Winnica DE, Kapralova VI, Kapralov AA, Tyurin VA, Kagan VE. LC/MS characterization of rotenone induced cardiolipin oxidation in human lymphocytes: implications for mitochondrial dysfunction associated with Parkinson's disease. Mol Nutr Food Res. 2013; 57:1410–1422. [PubMed: 23650208]
57. Jiang J, Stoyanovsky DA, Belikova NA, Tyurina YY, Zhao Q, Tungekar MA, Kapralova V, Huang Z, Mintz AH, Greenberger JS, Kagan VE. A mitochondria-targeted triphenylphosphonium-conjugated nitroxide functions as a radio-protector/mitigator. Radiat Res. 2009; 172:706–717. [PubMed: 19929417]
58. Ji J, Tyurina YY, Tang M, Feng W, Stolz DB, Clark RS, Meaney DF, Kochanek PM, Kagan VE, Bayir H. Mitochondrial injury after mechanical stretch of cortical neurons in vitro: biomarkers of apoptosis and selective peroxidation of anionic phospholipids. J Neurotrauma. 2012; 29:776–788. [PubMed: 21895519]
59. Ji J, Kline AE, Amoscato A, Samhan-Arias AK, Sparvero LJ, Tyurin VA, Tyurina YY, Fink B, Manole MD, Puccio AM, Okonkwo DO, Cheng JP, Alexander H, Clark RS, Kochanek PM, Wipf P, Kagan VE, Bayir H. Lipidomics identifies cardiolipin oxidation as a mitochondrial target for redox therapy of brain injury. Nat Neurosci. 2012; 15:1407–1413. [PubMed: 22922784]
60. Tyurina YY, Tyurin VA, Kaynar AM, Kapralova VI, Wasserloos K, Li J, Mosher M, Wright L, Wipf P, Watkins S, Pitt BR, Kagan VE. Oxidative lipidomics of hyperoxic acute lung injury: mass spectrometric characterization of cardiolipin and phosphatidylserine peroxidation. Am J Physiol Lung Cell Mol Physiol. 2010; 299:L73–85. [PubMed: 20418384]
61. Tyurina YY, Tungekar MA, Jung MY, Tyurin VA, Greenberger JS, Stoyanovsky DA, Kagan VE. Mitochondria targeting of non-peroxidizable triphenylphosphonium conjugated oleic acid protects mouse embryonic cells against apoptosis: role of cardiolipin remodeling. FEBS Lett. 2012; 586:235–241. [PubMed: 22210054]
62. Tyurina YY, Polimova AM, Maciel E, Tyurin VA, Kapralova VI, Winnica DE, Vikulina AS, Domingues MR, McCoy J, Sanders LH, Bayir H, Greenamyre JT, Kagan VE. LC/MS analysis of cardiolipins in substantia nigra and plasma of rotenone-treated rats: Implication for mitochondrial dysfunction in Parkinson's disease. Free Radical Res. 2015; 49:681–691. [PubMed: 25740198]
63. Tyurina YY, Kisin ER, Murray A, Tyurin VA, Kapralova VI, Sparvero LJ, Amoscato AA, Samhan-Arias AK, Swedin L, Lahesmaa R, Fadeel B, Shvedova AA, Kagan VE. Global phospholipidomics analysis reveals selective pulmonary peroxidation profiles upon inhalation of single-walled carbon nanotubes. ACS Nano. 2011; 5:7342–7353. [PubMed: 21800898]
64. R Development Core Team. R: A language and environment for statistical computing. R Foundation for Statistical Computing; Vienna, Austria: 2010.
65. Tyurin VA, Tyurina YY, Feng W, Mnuskin A, Jiang J, Tang M, Zhang X, Zhao Q, Kochanek PM, Clark RS, Bayir H, Kagan VE. Mass-spectrometric characterization of phospholipids and their primary peroxidation products in rat cortical neurons during staurosporine-induced apoptosis. J Neurochem. 2008; 107:1614–1633. [PubMed: 19014376]

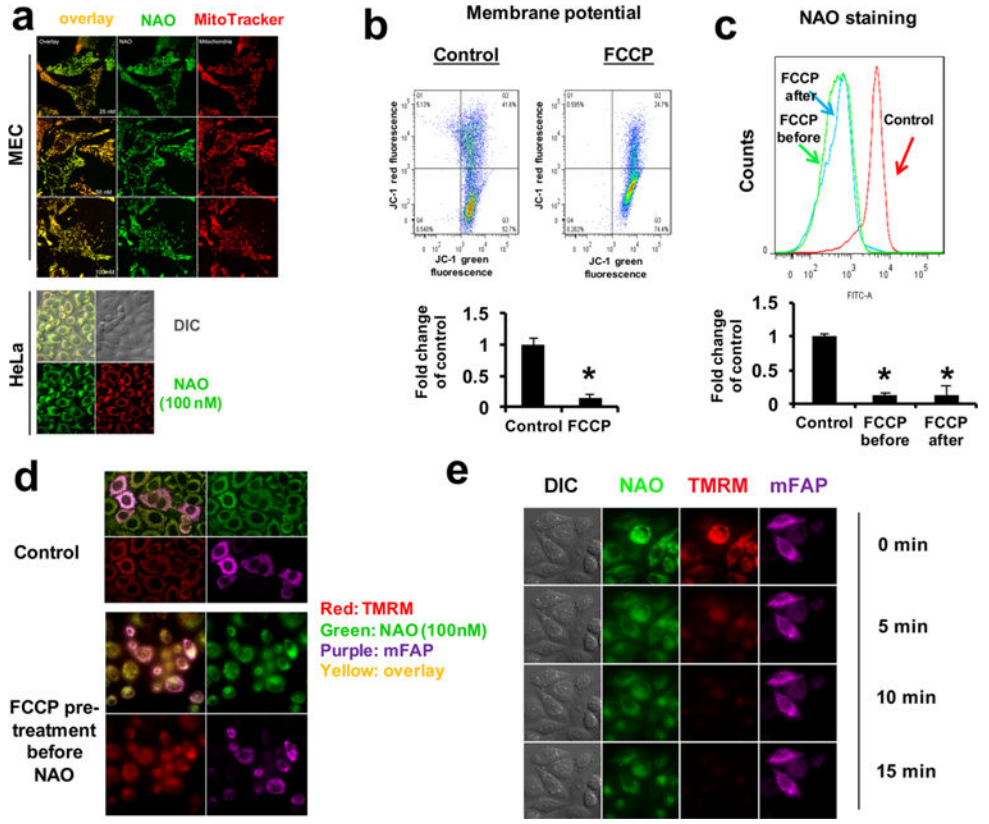


**Figure 1.**

Selective accumulation of NAO in mitochondria shown to be membrane-potential-dependent. (a) On the upper panel, MECs were incubated with NAO (25, 50, or 100 nM) and MitoTracker Deep Red (200 nM) for 30 min before imaging. On the lower panel, HeLa cells were treated the same way as MECs except NAO concentration was 100 nM, which was used for the following experiments. (b) Cells were pretreated with FCCP (40 $\mu$M) for 30 min before membrane potential was examined. Shown on the upper panel is the pseudocolor plot of JC-1 green versus red fluorescence in flow cytometry and on the lower panel are averaged quantitative assessments. (c) Cells were incubated with NAO for 30 min before light exposure (30 min). FCCP (40 $\mu$M) was added to cells either before (FCCP before) or after (FCCP after) NAO staining for 30 min prior to light exposure followed by the measurement of NAO staining. Shown on the upper panel are flow cytometry histograms of NAO staining, and on the lower panel are averaged quantitative results. (d) Cells infected with an adenoviral vector expressing mitochondrially targeted fluorogen activating protein (mFAP) were pretreated with vehicle control (upper panel) or FCCP (lower panel) for 30 min followed by the incubation with NAO and TMRM for 30 min before imaging. (e) Cells were treated similarly as in d except FCCP was given after NAO and TMRM treatments. Mitotracker (red), mFAP (purple), NAO (green), TMRM (red), and overlay (yellow). Mean ± SD ($N = 3$). *$p < 0.05$ vs controls.

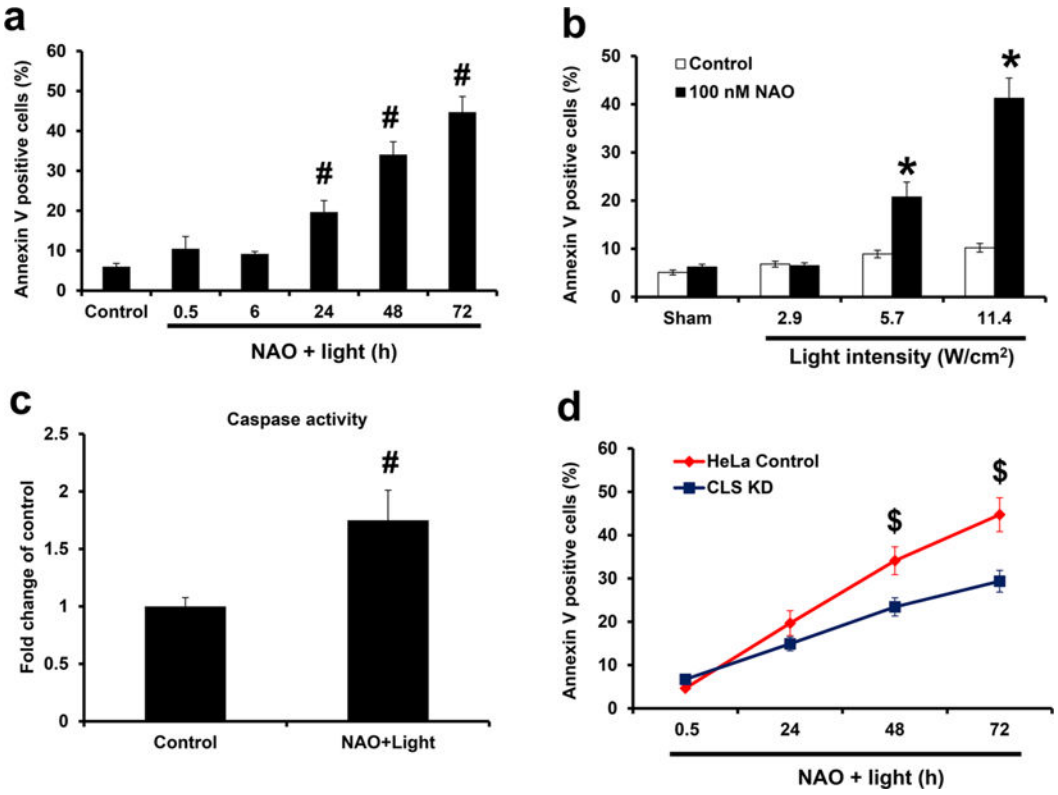


**Figure 2.**

NAO facilitating opto-activated apoptosis in a CL-dependent manner. (a) Cells were treated with NAO (100 nM) for 30 min and light exposure (5.7 W/cm$^2$) for 30 min, and PS externalization by Annexin V binding was analyzed at different time points (0.5, 6, 24, 48, and 72 h) after treatments. (b) Cells were treated with NAO for 30 min and exposed to light at different intensities (W/cm$^2$) for 30 min. At 24 h after treatment, cells were collected for analysis of PS externalization. (c) NAO-loaded cells were exposed to light as described in a, and caspase activity was measured at 24 h. (d) WT and CL-deficient (induced by CLS knockdown) HeLa cells were treated with NAO and light as described in a. Cells were collected at different time points (0.5, 24, 48, and 72 h) for analysis of PS externalization. CLS KD: cardiolipin synthase knockdown. Mean ± SD ($N$ = 3). $^{\#}p < 0.05$ vs nontreated controls. $^{*}p < 0.05$ vs light only treated controls; $^{\$}p < 0.05$ vs WT cells under the same conditions.

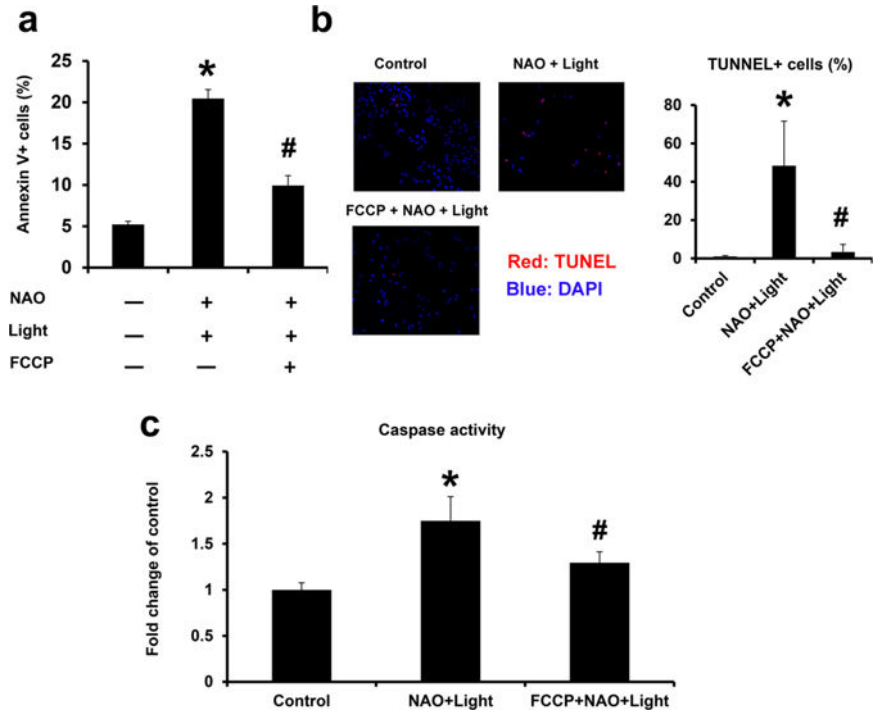


**Figure 3.**

FCCP shown to protect cells against apoptosis induced by NAO and light exposure. Cells were pretreated with 40 $\mu$M FCCP before NAO staining and light exposure. (a) Cells were collected for analysis of PS externalization by Annexin V binding at 24 h after treatments. (b) Cells were collected for analysis of TUNEL and DAPI staining at 48 h after treatments. Shown on the left panel are representative images from control, NAO + light, and NAO + light + FCCP groups. The red color is the TUNEL stain overlaid on the DAPI (nuclear) stain. Shown on the right are averaged quantitative results showing the number of TUNEL positive cells (normalized to the number of DAPI positive cells) in these three groups. (c) Measurement of caspase activity at 24 h after NAO and light exposures. Mean ± SD ($N = 3$). $^{*}p < 0.05$ vs nontreated controls. $^{\#}p < 0.05$ vs NAO and light treatments.

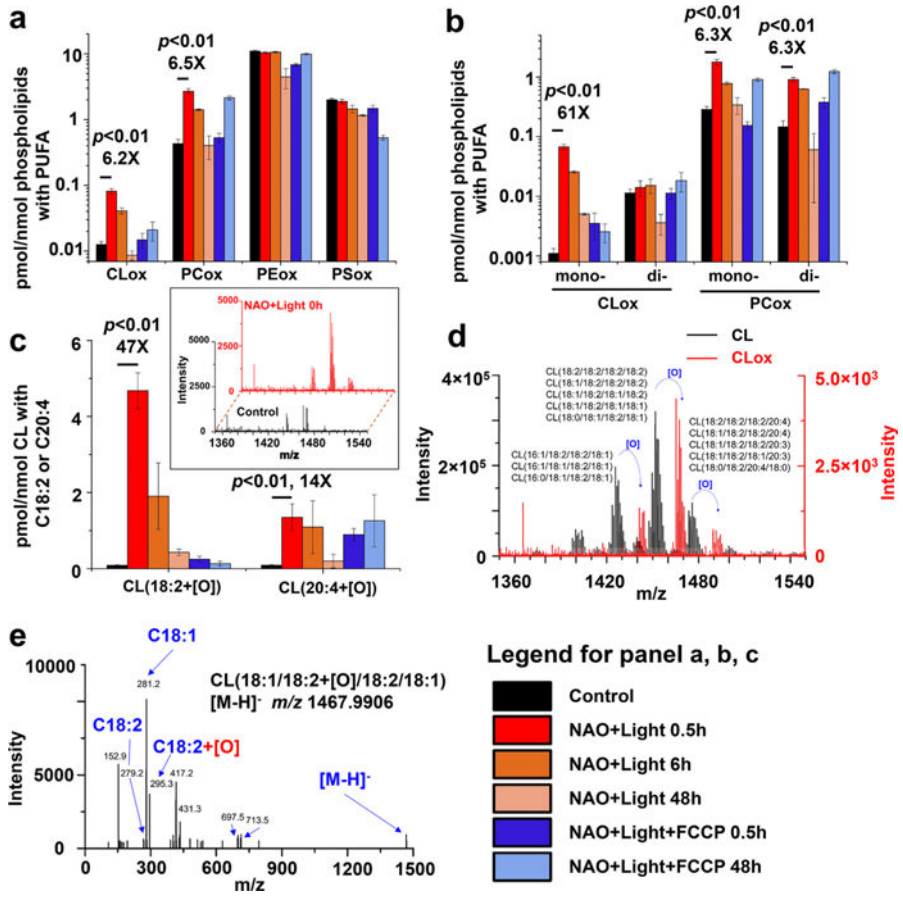


**Figure 4.**

Redox opto-lipidomics identifying C18:2 mono-oxygenated CL species as pro-apoptotic signals (a) Total levels of oxygenated PLs in HeLa cells following the exposure to NAO and light in the absence and presence of FCCP. The amounts of oxygenated species in major PL classes were normalized to the total contents of PLs with oxidizable polyunsaturated fatty acyls (PUFA). (b) Levels of mono-oxygenated CLs and PCs. The amounts of each oxygenated species were normalized to the total contents of PLs with oxidizable PUFAs. (c) The levels of mono-oxygenated CLs containing C18:2 or C20:4. The amount of each oxygenated species was normalized to the total contents of CLs with C18:2 and C20:4. Inset: Spectra of oxygenated CLs from control cells (black) and NAO + light exposed cells (red) collected immediately after the light. All values on panels a, b, and c are means ± SD ($N = 3$); also shown numerically are fold-changes induced by NAO + Light vs controls. (d) An overlay of a typical MS spectrum of nonoxygenated CL species from the control sample (black) and of oxygenated CL species (red) from the NAO + Light (0.5 h) sample (red) indicates the mono-oxygenated C18:2-containing CL species. Note the different scales on the black and red *y* axes of intensity. (e) Representative MS/MS spectrum of mono-oxygenated CL(18:1/18:2-[O]/18:2/18:1), with an *m*/*z* value of 1467.9906 ([M–H]$^-$).

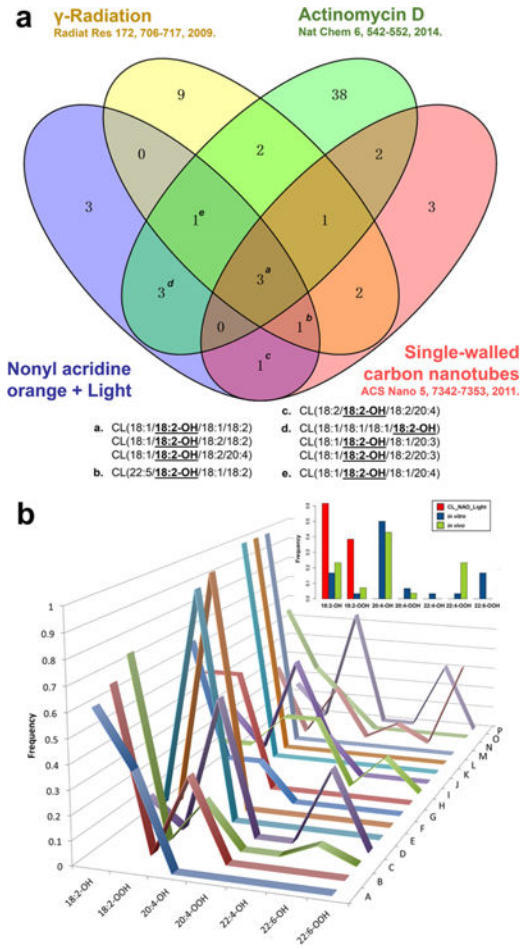


**Figure 5.**

Bioinformatics analysis verifying the commonality of mono-oxygenated C18:2 CL species as pro-apoptotic lipid signals. (a) The four-way Venn diagram demonstrates three mono-oxygenated C18:2 CL species common to the four different pro-apoptotic conditions. The Venn diagram was plotted using VENNY 2.0, http://bioinfogp. cnb.csic.es/tools/venny/. (b) Unigram frequencies of observed oxidized acyl chains upon apoptosis induction by different stimuli highlight mono-oxygenated C18:2 CL species. A, NAO-light (current work); B, actinomycin D (2012);[61] C, actinomycin D (2014);[19] D, controlled cortical impact;[19] E, gamma irradiation (2008);[22] F, gamma irradiation (2009);[57] G, gamma irradiation (2011, *in vitro*);[22] H, gamma irradiation (2011, *in vivo*);[22] I, hyperoxia;[60] J, mechanical injury;[58] K, actinomycin D (current work); L, rotenone (2013);[56] M, rotenone (2015);[62] N, staurosporine;[65] O, single walled carbon nanotubes;[63] and P, whole body radiation.[19] In the inset boxplot, the same frequencies are shown by grouping the stimuli as follows: NAO-light (this work) in red, *in vitro* (B, C, F, G, J, K, L, and N) in blue, and *in vivo* (D, E, H, I, M, O, and P) in green. The $p$ value of each comparison by $\chi$-squared test was shown in Supporting Information Table S2.

**Table 1**

Molecular Speciation of PLs in HeLa Cells

| abundance[a] (%) | CL | PC | PE | PS | PI | PG |
|---|---|---|---|---|---|---|
| >50% | | | | | PI(18:0/20:4) | PG(16:0/18:1) |
| 20–50% | | PC(16:0/18:1) | PE(18:0/20:4) | PS(18:0/20:4) | | |
| | | | | PS(18:0/18:1) | | |
| 5–20% | CL(18:1/18:2/18:1/18:2) | PC(16:0/20:4) | PE(P-18:0/20:4)[b] | PS(20:3/20:4) | PI(18:0/18:1) | |
| | CL(16:1/18:1/18:2/18:1) | PC(18:0/18:2) | PE(18:1/20:4) | PS(18:1/20:4) | PI(18:0/18:2) | |
| | CL(18:1/18:2/18:2/18:2) | PC(16:0/16:1) | PE(18:1/18:1) | | | |
| | CL(16:0/18:1/18:2/18:1) | PC(18:0/18:1) | PE(P-18:0/20:5) | | | |
| | CL(16:1/18:2/18:2/18:1) | PC(16:0/16:0) | PE(P-16:0/20:4) | | | |
| | CL(18:1/18:2/18:1/18:1) | PC(16:0/18:2) | | | | |
| | | PC(18:0/20:4) | | | | |
| | | PC(18:1/20:4) | | | | |
| 1–5% | CL(18:2/18:2/18:2/18:2) | PC(18:1/18:2) | PE(P-20:0/20:5) | PS(20:3/22:4) | PI(18:1/20:4) | PG(16:0/18:0) |
| | CL(16:0/18:1/16:0/18:1) | PC(O-18:1/16:0)[b] | PE(16:0/18:1) | PS(20:2/22:6) | PI(18:1/22:4) | |
| | CL(18:0/18:1/18:2/18:1) | PC(16:0/18:0) | PE(18:2/18:2) | PS(16:1/20:3) | PI(16:0/20:4) | |
| | CL(l8:1/18:2/18:2/20:3) | PC(14:0/16:0) | PE(P-18:0/22:4) | PS(18:0/22:4) | PI(18:0/22:4) | |
| | CL(l8:1/18:2/18:1/20:3) | PC(16:0/22:6) | PE(20:1/20:4) | PS(20:3/22:6) | PI(18:0/22:6) | |
| | CL(16:0/18:1/18:1/18:1) | PC(16:0/20:5) | PE(18:0/22:6) | PS(18:1/22:4) | PI(16:0/18:1) | |
| | CL(18:1/18:2/16:0/16:1) | PC(18:0/22:6) | PE(P-18:0/22:6) | PS(18:0/18:2) | | |
| | CL(16:1/16:1/18:2/18:1) | PC(20:1/20:4) | PE(18:0/22:4) | PS(16:0/18:1) | | |
| | CL(16:1/18:1/16:0/18:1) | PC(O-18:1/20:4) | PE(P-16:0/22:6) | | | |
| | CL(18:1/18:1/18:1/18:0) | | PE(16:0/22:6) | | | |
| | CL(16:1/18:2/18:2/18:2) | | PE(18:1/18:2) | | | |
| | CL(l8:1/18:2/18:2/20:4) | | PE(O-18:0/22:4) | | | |
| | CL(l8:1/18:2/18:0/20:3) | | PE(O-20:0/20:4) | | | |
| | CL(16:0/18:1/18:1/18:0) | | | | | |
| | CL(18:2/18:2/18:2/20:4) | | | | | |
| | CL(18:1/18:2/18:2/22:4) | | | | | |

[a]PLs were sorted by their abundance within corresponding subclass. Only phospholipipds with the abundance above 1% are shown, other compounds are in Supporting Information Table S1.

[b] P-, 1-(1Z-alkenyl),2-acylglycerophospholipids; O-, 1-alkyl,2-acylglycerophospholipids.